Journal of Theoretical and Applied Physics (JTAP), Vol.16, No. 1, 162204 (1-8), 2022
Received 15 January 2022; Accepted 8 February 2022; [http://dx.doi.org/10.30495/jtap.162204]

The interface of FeCrP film with graphene-like BN: electronic, band alignment, and thermoelectric properties

Mansoure Ilkhani*

Abstract
Based on the Density Functional Theory (DFT) and Generalized Gradient Approximation (GGA), the structural, electronic, and band alignment properties of the interface of FeCrP film with graphene-like BN (g-BN) were studied. These properties have been investigated at three different distances between FeCrP film and g-BN. In all three mentioned distances, the ground state point and the bulk modulus show that these compounds have the necessary strength to form, and at the distance of 2.7628 $\AA$, the compound is more stable than the other two distances. At this interface, the bulk modulus is greater than its values for the pure FeCrP and also the g-BN compounds. In addition, at the FeCrP-BN interface, the emergence of a large magnetic moment of 13.995 μ_B is found. Based on the mBJ approximation, this interface has a half-metallic characteristic and in the minority spin, it has a direct bandgap of 0.41 eV spin flip. At this interface, the Schottky height was obtained to be about 1.89 eV. It is found that the BN electronic structure is n-type and the E_{CNL}s appearing in this band alignment are close to the Fermi level as donor-like.

Keywords
FeCrP-BN interface, DFT, Electronic, Band alignment, Thermoelectric.

Department of Physics, Shahr-e-Qods Branch, Islamic Azad University, Tehran, Iran
***Corresponding author**: m.ilkhani@qodsiau.ac.ir

1. Introduction

Half-Heusler compounds (F-43m space group) comprise a relatively large family of materials with amazing physical properties and applications including the thermoelectric [1–3], piezoelectric [4], half-metallic [5], and topological properties [6, 7]. The half-metallic nature of NiMnSb half-Heusler compound was first reported by de Groot et al, in 1983. They showed that this case is metal at spin-up, and is semiconductor at another spin [8]. Since then, the computed electronic structures have shown many half-Heusler compounds to be half-metallic or nearly half-metallic, often with large band gaps because they have 100% spin polarization at the Fermi level and they can have relatively high Curie temperatures. However, many of the half-Heusler compounds have been predicted by half-metallic first-principles calculations [9–13], systematic studies of the electronic and magnetic properties of half-Heuslers are necessary to find which of them is stable. In addition, Half-Heusler (HH) alloys are one of the most promising structures in the field of thermoelectric materials (TE) intended for power generation at medium to high temperatures. The great advantage in the optimization of thermoelectric properties is the dimensionless figure of merit, the peak of which is ZT=1 and is even more than one in n-type materials [14]. The compatibility of thermoelectric materials with industrial applications requires in-depth knowledge of thermoelectric properties. In addition to efficient thermal power plant production or refrigeration capability for commercial use, mechanical strength can be mentioned as the applications of half-Heusler compounds [15–18]. Hexagonal boron nitride graphene (h-BN) has a crystalline structure with a 5.9eV energy gap, while in carbon graphene the energy gap is zero. Therefore, this two-dimensional structure has attractive electronic properties. Hexagonal boron nitride (h-BN) is the only phase structure of this compound with hexagonal configuration in all phases [19–22], which its structure is similar to the graphene layer, known as "white graphene". Each layer of this structure is made of a hexagonal lattice of B and N atoms. Due to the electronic properties of this compound, the BN Graphene has a great appeal in the electronics industry, as an oxidizing additive for refractory materials, as an insulator in the film of electronic devices, as a transparent insulator for electroluminescence devices with transparency in X-rays and visible areas, etc.

Band alignment of interfaces, defined by band offset of valence and conduction at common heterointerfaces, is technically important for the design and development of electronic, photovoltaic, photocatalytic devices, etc. [23–25]. These heterointerfaces include interfaces dipoles [26], which have a much smaller effect than surface dipoles due to their participation in interface chemical bonds. Among the three types of heterojunctions, band alignment type-II is very suitable

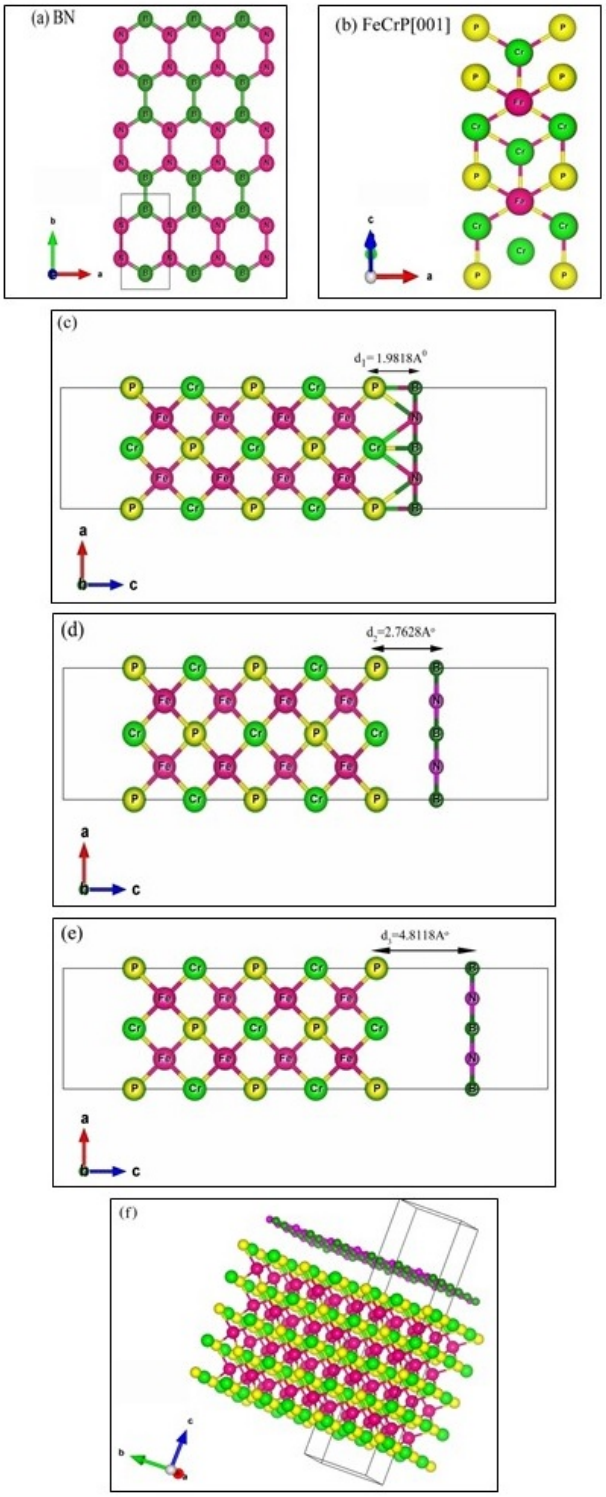

Figure 1. (a) The BN graphene cell, (b) the FeCrP [001] film, (d-f) various form of FeCrP-BN supercell.

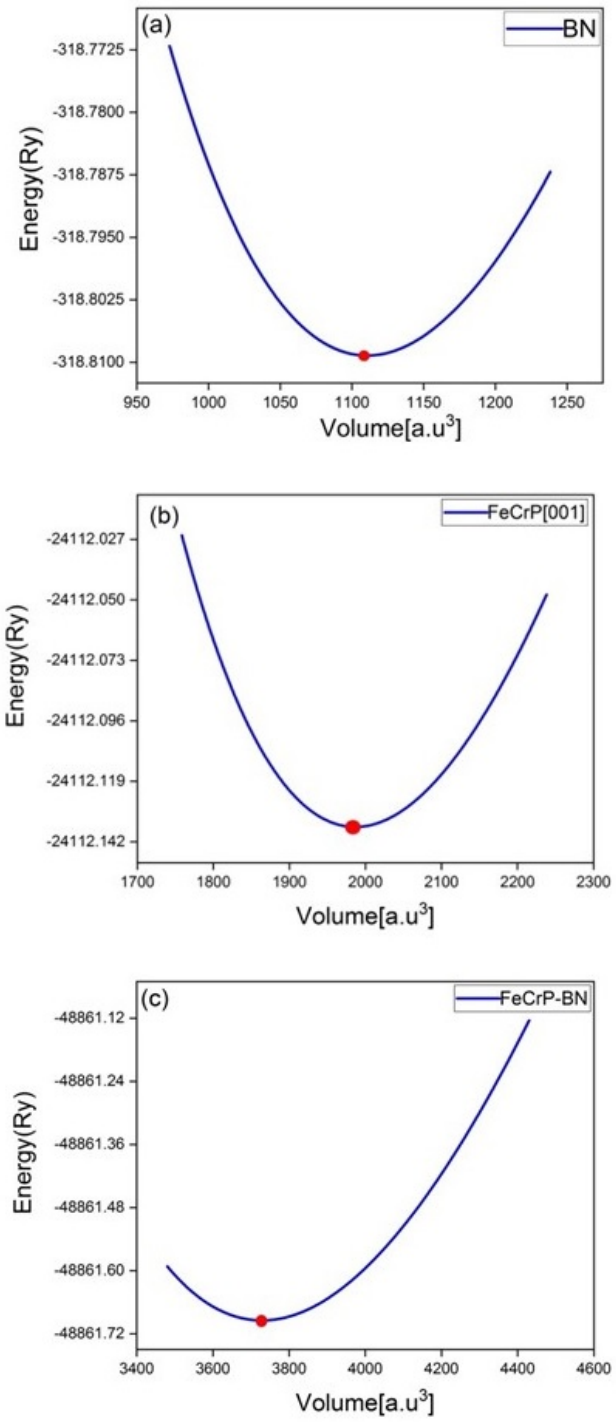

Figure 2. The energy-volume diagrams of (a) BN graphene like, (b) FeCrP [001] film, (c) FeCrP-BN supercell.(In all figures the ground state points are in red point).

to be employed in electronic unipolar devices because this type of band alignment creates a large offset on one side of the gap (conduction or valence bands), leading to a strong constraint on charge carriers. InAs/AlSb-based type-II electronic high-mobility transistors are a great example of these limitations [27]. These heterogeneous structures are also suitable for engineering the energy transfer from the conduction to the valence band. This issue is very important in tunnel

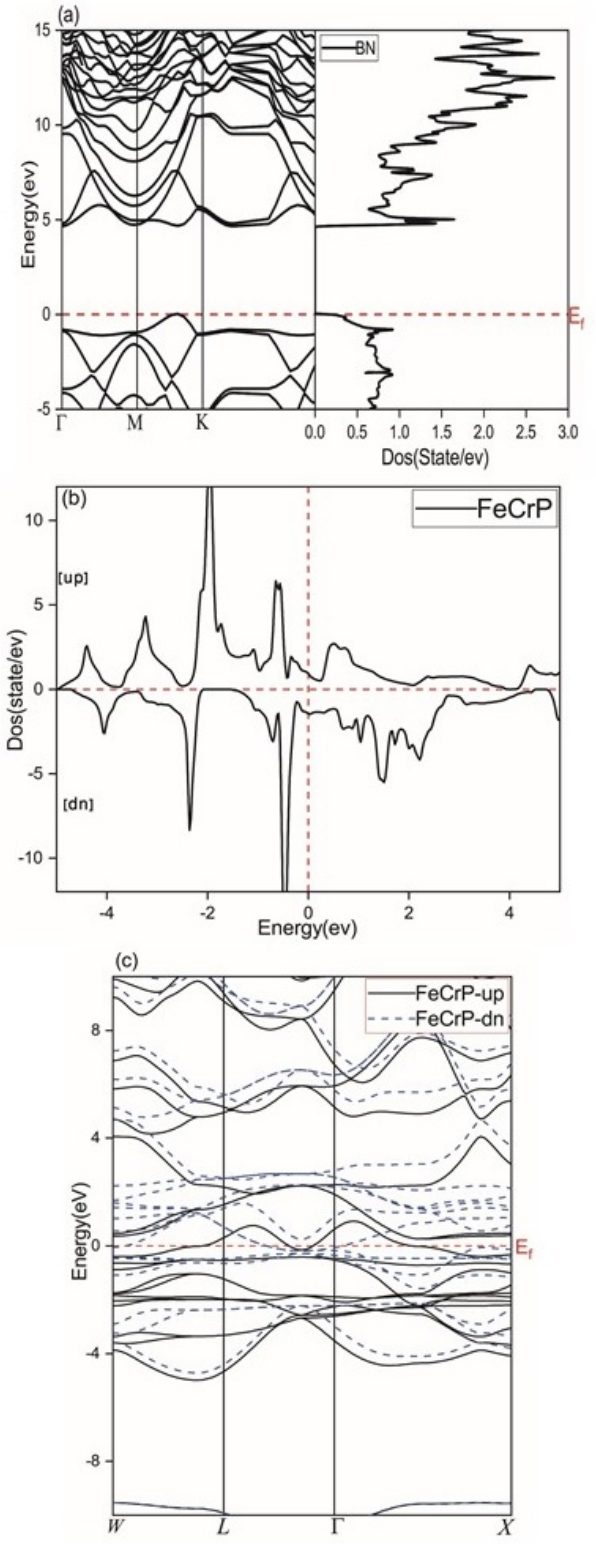

Figure 3. The DOS and bandstructure of (a) BN graphene like, (b) FeCrP.

field-effect transistors (TFETs) to escalate the tunneling current density [28]. They can also be used in sub-interband lasers of the infrared super lattice and wavelength optical detectors [29, 30].

2. Computational details

The Density Functional Theory (DFT) framework is employed to perform the first-principles calculations [31], in which the Kohn-Sham equations, one electron equations, can be extracted from the reduction many-body problem of interacting nuclei and electrons [32]. The full-potential linearized augmented plane wave (FP-LAPW) method [33] is applied to solve the Kohn-Sham equations which are used in the Wien2K package [34]. In addition, parameterization of the Perdew-Burke-Ernzerhof generalized gradient approximation (PBE-GGA) [35] is applied to calculate the exchange-correlation potential. Both up and down spin states are considered to carry out the spin-polarized calculations.

RMT=2.0 a.u is considered for all atoms as well as RK_{max}=8.0, L_{max}=10, and G_{max}=12 $(a.u)^{-1}$. Moreover, -8 Ry is considered for the cutoff energy which separates the core and valence electrons, and a $12\times12\times2$ grid is considered in the irreducible Brillouin zone. The energy and charge convergence tolerance are taken to be 10^{-4} Ry and10^{-4} electrons in the self-consistent calculations, respectively. To calculate the thermoelectric properties, the BoltzTraP code is used.

3. Results and discussions

As can be seen in Figure 1, BN armchair graphene has a hexagonal geometry. In this figure, the selected BN graphene cell is identified, which creates the graphene by expanding it. Regarding the interface of BN graphene with any selected substrate, the geometric consistency of the substrate with the BN graphene structure is important. For this reason, the FeCrP thin film in the [001] direction is chosen because the cross-section of the FeCrP [001] supercell is also cubic, so it has the highest compatibility with the selected cell with BN armchair graphene. The presence of Cr atoms on the surface and Fe in the layer below the surface of the FeCrP film in panel (c) causes the presence of electrons of their half-filled d orbitals on the substrate surface. Accordingly, these electrons cause high activity in terms of finding new properties that can be found between BN graphene and the substrate.

To start the calculations, it is necessary to optimize the crystal structure of the substrate and the film. Thus, the volumes of FeCrP film [001], g-BN cells, and FeCrP-BN supercell are optimized and the equilibrium volume is determined according to Figure 2 at the ground state point. As can be seen from these figures, all three curves have a minimum point, so it is possible to find an equilibrium volume for them, either in the pure state or in the interface state, whose structural coordinates include lattice constants, bulk modulus, bulk modulus derivative, equilibrium volume, total energy and total magnetic moment are listed in Table 1. All energy-volume graphs

Table 1. Lattice constants a, b, and c (Bohr), equilibrium volume of cell (a.u.^{3}), bulk modulus B(GPa), derivative of bulk modulus B, total energy (Ry), total magnetic moments of BN graphene like, FeCrP[001] film, and FeCrP-BN

Parameter	a_{bohr}	b_{bohr}	c_{bohr}	Volume[a.u.^{3}]	B(GPa)	B	Energy(Ry)	$M_{tot}(\mu_B)$
BN	4.75216	8.232537	28.3880	1110.6074	52.2927	3.6478	-318.809210	0.0
FeCrP[001]	7.401326	7.401326	41.87522	1986.5837	100.6582	4.2803	-24112.136394	4.9117
FeCrP-BN	10.23526	10.23526	41.09828	3729.1876	163.7159	3.2944	-48861.694470	13.9954

in Figure 2 are in ferromagnetic modes.

Calculations demonstrate that by adding the g-BN layer to the FeCrP [001] thin film, the bulk modulus has increased by about 63%, indicating that there is a strong tendency to combine between the FeCrP [001] film and the g-BN layer. In FeCrP films, the bulk modulus derivative is larger than the bulk modulus derivative of FeCrP-BN. As can be seen from the number, the bonds are ionic within the film while all bonds have found a covalent tendency in the presence of the g-BN layer and the formation of a Van der Waals bond between BN and FeCrP. The interesting point in Table 1 is that the FeCrP film has a magnetic moment of about 5 μ_B in the pure state. On the other hand, the BN layer does not have a magnetic moment in its pure state, but at the interface of these two magnetic moments, FeCrP-BN is almost tripled, indicating how much the magnetic charge of this interface increases the magnetic moment of this interface due to this hexagonal BN and the formation of Van der Waals bond. The presence of the BN layer on this thin film leads to the formation of the Van der Waals bonds. In order to find the optimized distance of FeCrP film with BN graphene, the total energy of the FeCrP-BN supercell is calculated with a Van der Waals switch at different distances of d_1, d_2, and d_3 which are listed in Table 2. It is observed that the total crystal energy of this heterojunction at the d_2 distance is lower and it has greater stability from an energy point of view. Hence, the d_2 distance is considered as the optimal distance for the following calculations.

Table 2. The total energy of FeCrP-BN supercells for various mentioned distances.

distance	Energy(Ry)
d_1=1.9818 $\AA$	-48861.74528401
d_2=2.7628 $\AA$	-48862.11051859
d_3=4.8118 $\AA$	-48862.0974272

4. Electronic properties

In this section, the electronic properties of the FeCrP-BN interface are discussed. Understanding the electronic structure of materials is essential in knowing the physical understanding of materials. For this reason, two important tools are utilized called density of states (DOS) and band structure. For this purpose, the DOS and band curves in Figure 3 are first observed on BN graphene which BN is a P-type semiconductor with an indirect bandgap of 4.65 eV which is in good agreement with other previous works. As it is clear, the presence of intersected levels in the regions of valence and conduction, high density, and the continuity of electron states in the DOS curve make this graphene compound a very suitable option for electron transport and band alignment applications. In Figures (b) and (c), the DOS and band diagrams of the FeCrP [001] thin film are plotted in two spins of up and down which these calculations are based on the GGA approximation. It is observed that in the area of Fermi level, there is electron anisotropy expressing that this thin layer has half-metallic properties. The band structure illustrates that the high gradients of levels above the Fermi level in the first Brillouin zone make this film a good choice for electron sources. In Figure 4, the DOS curve of FeCrP-BN is plotted with two approximations of GGA and mBJ. It is observed that the FeCrP properties have witnessed significant changes in the interface of BN graphene with FeCrP. Using the GGA approximation, 95% spin polarization is observed and using the mBJ approximation, 100% spin polarization is detected. In panels (a) and (b), there are large spin polarization and strong half-metallic behavior. Applying the mBJ approximation causes a spin-flip gap of about 0.6 eV at the down spin. The high continuity of the DOS curves in both approximations represents that very high electron conductivity can be seen at this interface. In panel (c), the roles of the d orbitals of the Fe and Cr atoms and to some extent the p orbitals of the P atom are appeared to be in determining the Fermi level anisotropy and the formation of the magnetic moment of 13.66 μ_B, so the high-potential interface of the half-metallic behavior can be detected for this compound. The DOS diagrams in the conduction and valence regions, in both approximations, indicate that the excited electrons and holes participate well in the transport, and this interface can be a good candidate for spin electron injection, due to the spin polarization at the Fermi surface and the suitable spin-flip gap.

In Figure 5, the band structure diagrams of this interface are plotted in two spins of up and down with two approximations of GGA and mBJ. The common point in both diagrams in the down spin is the split of the levels at the Fermi level, which the three levels touch each other in the GGA approximation, but a direct gap of 0.41 eV is seen in the mBJ approximation.

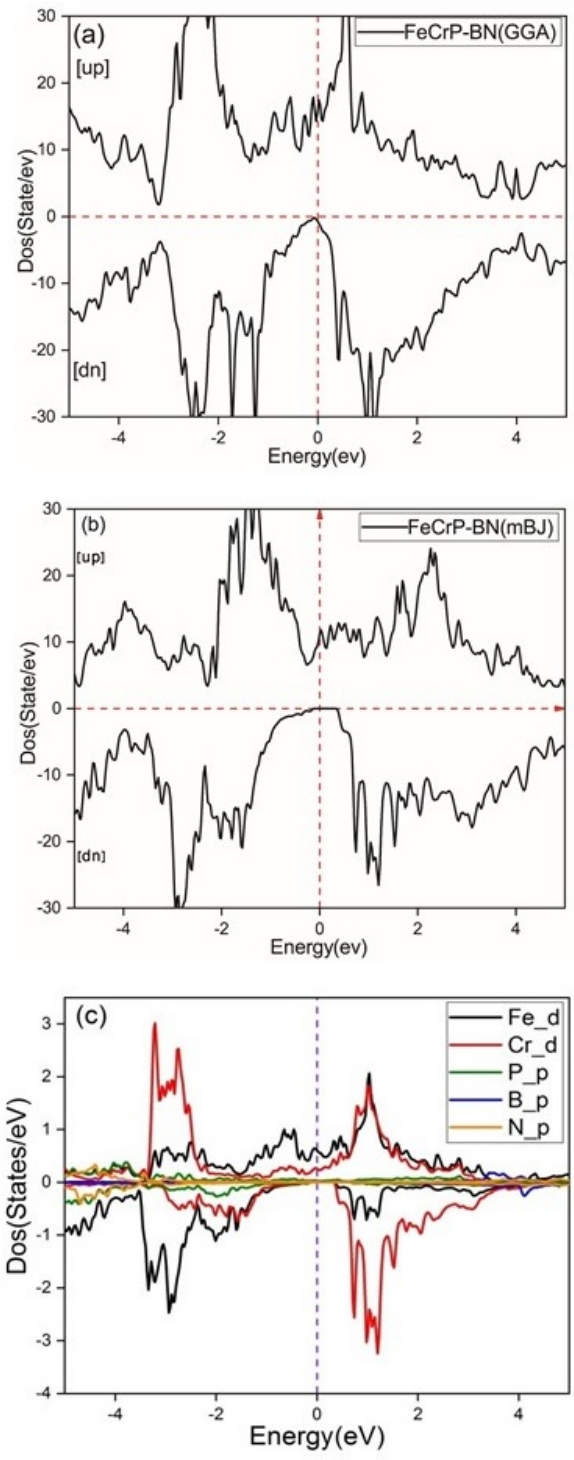

Figure 4. The DOS and bandstructure of FeCrP-BN interface (a, b) and Partial DOS, by GGA, and mBJ approximations.

The very high density of states around the Fermi level in the down spin makes this compound a good candidate for thermoelectric purposes. In the conduction region, it can be seen that the highest gradient of the bands occurs in the M direction.

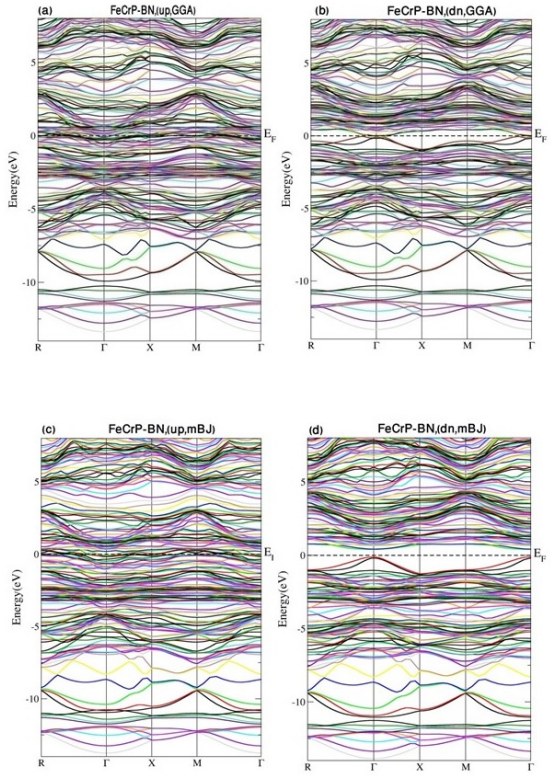

Figure 5. The bandstructure of FeCrP-BN interface with GGA and mBJ approximations in up and down spins.

The electron density of the FeCrP film [001] and the FeCrP-BN interface are plotted in Figure 6 in the up and down spins. In panels (a) and (b), it is obvious that P atoms are present at the selected FeCrP surface, where there is a relatively large high electron density near the surface, but no changes in electrical polarization with the change in spin are observed in these two spins. At the base, Fe and Cr atoms have the highest electron density and the bond between them is ionic. It is observed in panels (c) and (d) that with the addition of BN graphene, a change in electrical polarization is witnessed at the surface of the films. As it can be seen, the charge density of the BN graphene-like and the film, shown in green, displays that the bond between the atoms is weaker than the bonds between the atoms in the film which is of the Van der Waals type. It is also clear that the emergence of a charge density gradient and a change of those interface layers can be detected by changing the direction of the magnetic field from up to down. These changes occur mostly in the film region, indicating that the main cause of magnetic anisotropy is the Fe and Cr atoms, confirming the DOS and band curves. In the following, the electrostatic potential figure is illustrated in Figure 7, which is calculated for the film surface layer and the graphene-like BN surface. The depth of this potential at the film surface is almost twice that of the BN graphene-like

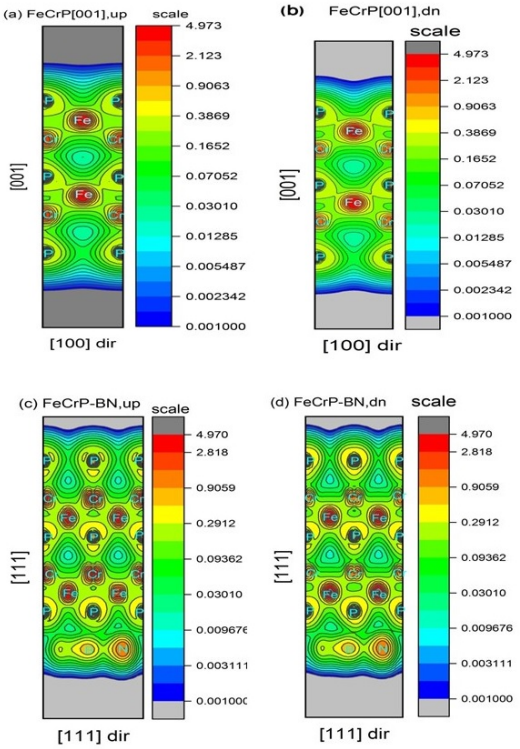

Figure 6. The Electron Density of the FeCrP [001] film and FeCrP-BN interface in up and down spins.

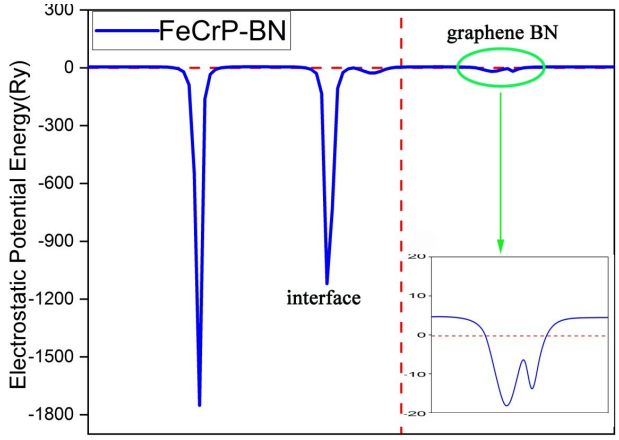

Figure 7. The electrostatic potential of the FeCrP-BN interface.

surface, indicating that this interface is a good option for a potential layer as well as a good candidate for injecting electrons from the FeCrP-BN film.

Figure 7 shows the electrostatic potential of this interface in the [001] direction. It can be seen the large electrostatic potential at interface difference of an order of 160 between these two layers. This large potential difference in electrostatic potential causes a force to be applied to the surface of graphene and film, and therefore the geometry of the density of free electrons in their surfaces are disturbed, resulting in electronic multipolarity and magnetic behavior. This potential difference, as shown in Figure 7, has led to a greater tendency of the film electrons towards the surface at the spin-dn, and the effects of the presence of g-BN in the vicinity of the film on the other level of the film are quite evident. This large potential difference is also quite evident in the Band alignment diagram of Figure 8 in the emergence of the work function and the parameters φ_B, CBM, and VBM.

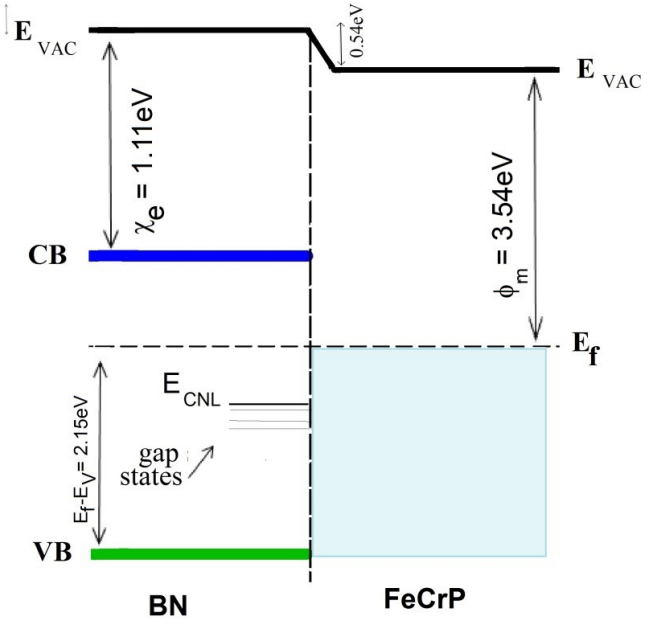

Figure 8. Band alignment diagram based on DFT calculations of BN-FeCrP heterojunction.

5. Band alignment

Band offset is a parameter affecting the transport of charge carriers in electrical junctions and measuring the exact amount of this deviation (VBO and CBO) which is essential in order to understand the relationship between the physical structure of the interface, its electronic structure, and charge transport. One of these types of electrical junctions is a semiconductor/metal junction. According to the Schottky model [36], when a semiconductor or insulator (dielectric) and a metal form an interface, the charge transfer at this boundary will not be possible due to the Schottky barrier (φ_B) over the electrons. This barrier appears in the vacuum due to the difference between the working function of the metal (φ_m) and the electron affinity (χ_e) of the semiconductor. Schottky height controls electron transport at the boundary, so it is of great importance in the performance of semiconductor devices. The small amount of Schottky height causes charge leakage, which is considered undesirable for the performance of the devices. Experience has shown that the Schottky model for measuring

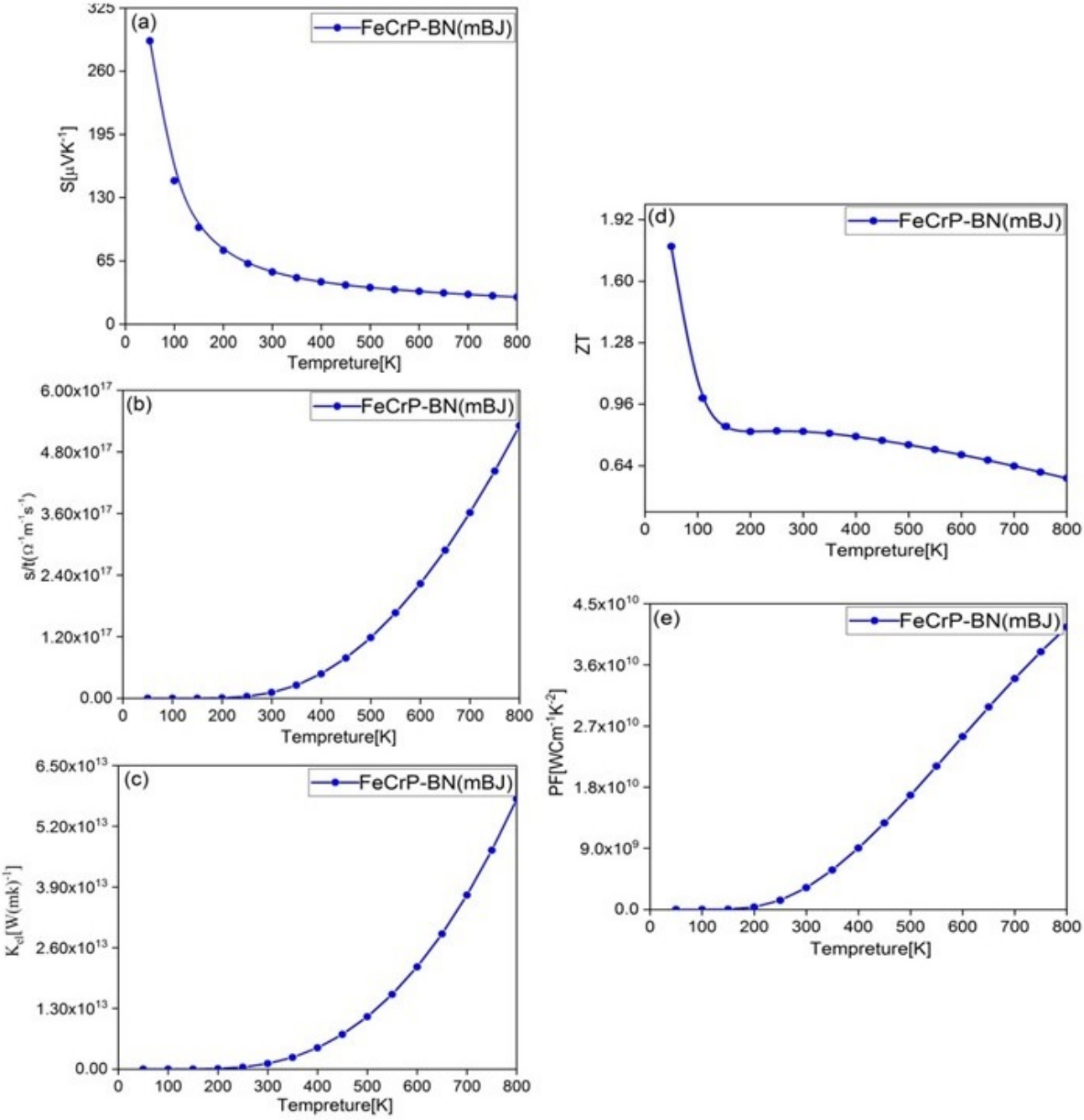

Figure 9. The thermoelectric coefficient of FeCrP-BN interface.

the height of a barrier is not very successful, so the model proposed by Bardeen [37] replaced it. The Bardeen model follows the Fermi-level pinning hypothesis. In this model, a surface density of states is considered for the edge of the conduction band, and it is assumed that these states pin the Fermi surface. Of course, this model was not very successful either, because for most metal/semiconductor boundaries this density of states does not appear in the semiconductor gap, so Heine [38] proposed a better hypothesis.

In the energy range that the bandgap of the semiconductor and the metal conduction band overlap, the electron wave functions in the metal pursue or fade into the semiconductor.

Table 3. Calculated data on metal work function(ϕ_m), VBM, CBM, ECNL, electron affinity (χ_e) and barrier heights(ϕ_B) at FeCrP–BN interface.

Heterojunction	ϕ_B (eV)	ϕ_m (eV)	χ_e (eV)	E_{CNL} (eV)	VBM-BN (eV)	CBM-BN (eV)
FeCrP/BN	1.89	3.54	1.11	-0.7408	-2.66	2.15
Mg/Al2O3 [67]	2.6	3.6	—	—	—	—
FeCrP/BN	1.9	4.7	—	—	—	—

These states in the bandgap are known as metal-induced gap states or intrinsic states [**?**, 39]. The presence of these metal-induced gap states at the metal/semiconductor or metal/insulator (dielectric) interface was also predicted by Louie and Cohen [40] using quasi-potential self-consistent calculations for the electronic structure of the material interface. Experimentally, these states were observed by Muller et al. with electron energy dissipation spectroscopy [41]. These states usually appear in the form of donor-like near the valence band or acceptor-like in the vicinity of the conduction band. The energy levels of these states located in the band gap are known as charge neutrality levels (E_{CNL}) depending on whether they are acceptor-like or donor-like [42, 43]. According to the above, the value of Schottky height can be calculated from the following equation:

$$\phi_B = S(\phi_m - E_{CNL}) + (E_{CNL} - \chi_e) \tag{1}$$

where S is the dimensionless factor of Schottky barrier pinning, obtained from the following relation in terms of dielectric constant [44]. Materials with S less than one tend to pin the metal Fermi level to the E_{CNL} level , while as this number approaches one, i.e. the maximum value of S, no pinning occurs for the Fermi level.

$$S = \frac{1}{1 + 0.1(\varepsilon_\infty - 1)^2} \tag{2}$$

In the present work, FP-LAPW self-compatible calculations based on DFT is used to study the FeCrP-BN interface. The results obtained for the band alignment of this interface in Figure 8 demonstrate that this is a type-I heterojunction [45–47]. The calculated values of the FeCrP work function, E_{CNL}, for BN are listed in Table 3. The Schottky height obtained at this interface is about 1.89 eV. As can be seen, the BN electronic structure is n-type and the E_{CNL}s appearing in this band alignment are close to the Fermi level as donor-like.

6. Thermoelectric

The current production in a conductor owing to the temperature difference between two points is called the thermoelectric effect. Thermoelectric effects are used to generate electricity, measure temperature, and cool objects. This phenomenon includes the Seebeck effect, which was first discovered by the German scientist Thomas Johann Seebeck in 1811. Seebeck performed experiments with different metals and concluded that the temperature difference in a circuit causes the charge carriers to move from hot to cold, so it creates an electric field and potential difference [48]. The Seebeck coefficient of a material is the magnitude of an induced thermoelectric voltage that depends on the temperature and crystal structure. The Seebeck coefficient sign expresses the type of charge carriers in electrical transport. In the n-type semiconductor, in which charge carriers are the electron, the Seebeck coefficient is negative, and in the p-type semiconductor, which charge carriers are the holes, the Seebeck coefficient is positive. The large Seebeck coefficient reveals that a small temperature difference creates a large voltage on both sides of the material, so a large Seebeck coefficient is necessary for a thermoelectric material. The thermoelectric efficiency of materials can be measured by calculating the dimensionless figure of merit, ZT, as well as the power factor that can be calculated using the following formula.

$$ZT = \frac{s^2 \sigma T}{K} \tag{3}$$

$$PF = S^2 \sigma \tag{4}$$

where T is the absolute temperature, S is the Seebeck coefficient, σ is the electrical conductivity and K is the thermal conductivity, including the lattice and electron contributions ($K = K_{el} + K_{latt}$) [49–52].

In figure 9, some important thermoelectric parameters are drawn for the FeCrP-BN interface. As it can be seen from the DOS and band structure, this compound is a p-type semiconductor in the down spin, so the sign of the Seebeck coefficient in all temperature ranges is positive, indicating that the charge carriers at this interface are of the holes. The highest amount of Seebeck coefficient occurs at temperatures below 100 K, which decreases by increasing temperature to 200 K and it continues to decline with a slow slope, afterward. In panel (b), this heterojunction is observed to have insignificant electrical conductivity up to room temperature, but the electrons pass through the bandgap from room temperature onwards, and the electric current in this interface is established with a steep slope. The same thing happens with thermal conductivity (see panel (c)). In panel (d), the dimensionless figure of merit is claimed to reach an amazing number of 1.8 at 50 K, indicating that this compound can be a good option in this temperature range for thermoelectric purposes such as cooling. By increasing temperature up to 100 K, the value of ZT has decreased

with a steep slope to reach an acceptable value of one. It is noteworthy that this diagram experiences stable conditions as the temperature rises and reaches room temperature to remain in the range of 0.8, so this compound can be considered as a thermoelectric candidate at room temperature. In panel (e), the power factor curve is plotted. It is zero up to 200 K, but the amount of power factor escalates with a steep slope by increasing temperature. Therefore, it can be claimed that the amount of power factor increases at high temperatures, so it can be concluded that this compound is a very good option for power generator applications.

7. Conclusion

The structural, electronic, band alignment and thermoelectric properties of the interface FeCrP Heusler film with Graphene-like BN was investigated based on density functional theory. Calculations were performed at three distances of 1.9818$\AA$, d_2=2.7628 $\AA$ and d_3=4.8118 $\AA$. Structural calculations showed that distance d_2 was more stable than other distances. The crystal hardness of the FeCrP-BN interface compound is higher than FeCrP, and Graphene-like BN compounds, and this interface has made the crystal hardness.

According to the mBJ approximation, this interface has half-metallic behavior with 100% spin polarization is at Fermi level, and a 0.41 eV direct energy gap at down spin. The proximity of the BN layer to the surface of the FeCrP film has caused an increase in the electron density gradient at the interface, which has led to the formation of electrical multi-polarity and is effective in electron transfer. Also, The Schottky height obtained at this interface is about 1.89 eV. As can be seen, the BN electronic structure is n-type and the E_{CNL}s appearing in this band alignment are close to the Fermi level as donor-like.

Conflict of interest statement:

The authors declare that they have no conflict of interest.

References

[1] A. Boochani, M. Jamal, M. Shahrokhi, B. Nowrozi, M. B. Gholivand, J. Khodadadi, E. Sartipi, M. Amiri, M. Asshabia, and A. Yaria. *J .Mater. Chem. C*, **7**:13559, 2019.

[2] J. Ma, V. I. Hegde, K. Munira, Y. Xie, S. Keshavarz, D. T. Mildebrath, C. Wolverton, A. W. Ghosh, and W. H. Butler. *Phys. Rev. B*, **95**:024411, 2017.

[3] J. R. Sootsman, D. Y. Chung, and M. G. Kanatzidis. *Angewandte Chemie International Edition*, **48**:8616, 2009.

[4] A. Roy, J. W. Bennett, K. M. Rabe, and D. Vanderbilt. *Phys. Rev. Lett.*, **109**:037602, 2012.

[5] D. Kieven, R. Klenk, S. Naghavi, C. Felser, and T. Gruhn. *Phys. Rev. B*, **81**:075208, 2010.

[6] W. Feng, D. Xiao, Y. Zhang, and Y. Yao. *Phys. Rev. B*, **82**:235121, 2010.

[7] S. Chadov, X. Qi, J. Kübler, G.H. Fecher, C. Felser, and S.C. Zhang. *Nature Materials*, **9**:541, 2010.

[8] R. B. Helmholdt, R. de Groot, F. Mueller, P. van Engen, and K. Buschow. *Journal of Magnetism and Magnetic Materials*, **43**:249, 1984.

[9] K.S. Novoselov, A.K. Geim, S.V. Morozov, D. Jiang, Y. Zhangs, V. Dubonsi, V. Grigorieva, and A. A. Firsov. *Science.*, **306**:666, 2004.

[10] X. Li, W. Cai, J. An, S. Kim, J. Nah, D. Yang, R. Piner, A. Velamakannii, E. Tutuc, S. K. Banerjee, L. Colombo, and R. S. Ruoff. *Science.*, **324**:1312, 2009.

[11] J. H. Chen, C. Jang, S. Xiao, M. Ishigami, and M. S. Fuhrer. *Nature Nanotechnology.*, **3**:206, 2008.

[12] M. Corso, W. Auwärter, M. Muntwiler, A. Tamai, T. Greber, and J. Osterwalder. *Science.*, **303**:217, 2004.

[13] M. Morscher, M. Corso, T. Greber, and J. Osterwalder. *Surface Science*, **600**:3280, 2006.

[14] A. Yari, A. Boochani, and S. Rezaee. *Philosophical Magazine*, **100**:3108, 2020.

[15] H. H. Xie, J.L. Mi, L.P. Hu, N. Lock, M. Chirstensen, Ch. G. Fu, B. B. Iversen, X. B. Zhaoa, and T.J. Zhu. *Cryst. Eng. Comm*, **14**:4467, 2012.

[16] K. Kirievsky, Y. Gelbstein, and D. Fuks. *J. Solid State Chem.*, **203**:247, 2013.

[17] Y. Gelbstein, N. Tal, A. Yarmek, Y. Rosenberg, M. P. Dariel, S. Ouardi, B. Balke, C. Felser, and M. Köhne. *J. Mater. Res.*, **26**:1919, 2011.

[18] M. Gürth, G. Rogl, V.V. Romaka, A. Grytsiv, E. Bauer, and P. Rogl. *Physica B: Cond. Mat.*, **104**:210, 2016.

[19] J. J. Pouch and S.A. Alterovitz. *Mater Manufacturing Process.*, **6**:373, 1991.

[20] R. Haubner, M.Wilhelm, R. Weissenbacher, and B. Lux. *synthesis and applications.*, **6**:1539, 2008.

[21] X. Gao, Z. Zhou, Y. Zhao, S. Nagase, S.B. Zhang, and Z. Chen. *J Phys Chem C.*, **112**:12677, 2008.

[22] Sun P Ding Y Li Y Ma F. ; Wang J, Cao S. *RSC Adv.*, **6**:111345, 2016.

[23] D. Cahen and A. Kahn. *Advanced Materials.*, **15**:271, 2003.

[24] S.J. Moniz, S.A. Shevlin, D.J. Martina, Z.X. Guo, and J. Tang. *Energy and Environmental Science.*, **8**:731, 2015.

[25] J. Robertson. *Journal of Vacuum Science and Technology A: Vacuum, Surfaces, and Films.*, **31**:050821, 2013.

[26] A. Franciosi and C.G. Van de Walle. *Surface Science Reports.*, **25**:1, 1996.

[27] J.D. Werking, C.R. Bolognesi, L.D. Chang, C. Nguyen, E.L Hu, and H. Kroemer. *IEEE electron device letters*, **13**:164, 1992.

[28] S.O. Koswatta, S.J. Koester, and W. Haensch. *IEEE Transactions on electron devices*, **57**:3222, 2010.

[29] J.R. Meyer, C.A. Hoffman, F.J. Bartoli, and L.R. Ram-Mohan. *Applied physics letters.*, **67**:757, 1995.

[30] Y. Zhang, W. Ma, Y. Cao, J. Huang, Y. Wei, K. Cui, and J. Shao. *IEEE Journal of Quantum Electronics.*, **47**:1475, 2011.

[31] W. Kohn, A.D. Becke, and R.G. Parr. *J.Phys. Chem.*, **100**:12974, 1996.

[32] W. Kohn and L.J. Sham. *Phys. Rev.*, **140**:1133, 1965.

[33] P. Blaha, K. Schwarz, P. Sorantin, and S. Trickey. *Phys. Commun.*, **59**:2399, 1990.

[34] P. Blaha, K. Schwarz, G. Madsen, D. Kvasnicka, and J. Luitz. *wien2k, An augmented plane wave+ local orbitals program for calculating crystal properties.* Inst. of Physical and Theoretical Chemistry Getreidemarkt, 7th edition, 2014.

[35] J.P. Perdew, K. Burke, and M. Ernzerhof. *Phys. Rev. Lett.*, **77**:3865, 1996.

[36] W. Schottky. *Zeitschrift für Physik*, **118**:539, 1942.

[37] J. Bardeen. *Physical Review.*, **71**:717, 1947.

[38] V. Heine. *Physical Review.*, **138**:1689, 1965.

[39] W. M¨onch. *Surface science*, **299**:928, 1994.

[40] S.G. Louie and M.L. Cohen. *Physical Review B.*, **13**:2461, 1976.

[41] D.A. Muller, D.A. Shashkov, R. Benedek, L.H. Yang, J. Silcox, and D.N. Seidman. *Physical review letters.*, **80**:4741, 1998.

[42] C. Tejedor, F. Flores, and E. Louis. *Journal of Physics C: Solid State Physics.*, **10**:2163, 1977.

[43] J. Tersoff. *Physical Review B.*, **32**:6968, 1985.

[44] W. M¨onch. *Electronic Properties of Semiconductor Interfaces*. Springer, 1th edition, 1988.

[45] A.A. Demkov. *Physical Review B.*, **74**:085310, 2006.

[46] I. Razdolski, A.L. Chekhov, A.I. Stognij, and A. Stupakiewicz. *Physical Review B.*, **100**:045412, 2019.

[47] J. Robertson. *Physica status solidi (a)*, **207**:261, 2010.

[48] V.B. Bobrov, S.A. Trigger, G.J.F. Van Heijst, and P. P. J. M. Schram. *Europhysics Letters Association*, **90**:10003, 2010.

[49] S.D. Guo and L. Qiu. *J. Phys.D Appl. Phys.*, **50**:015101, 2017.

[50] D.K. Ko, Y.J. Keng, and C.B. Murray. *Nano Lett.*, **11**:2841, 2011.

[51] L. Muchler, F. Casper, B. Yan, S. Chadov, and C. Felser. *Phys. Status Solidi RRL.*, **7**:91, 2013.

[52] Y.V. Ivanov, A.T. Burkov, and D.A. Pshenay-Severin. *Phys. Status Solidi B.*, **255**:1800020, 2018.